An alternative active site architecture for O_2 activation in the ergothioneine biosynthetic EgtB from *Chloracidobacterium thermophilum*

Anja R. Stampfli[1,2], Kristina V. Goncharenko[1], Marcel Meury[1], Badri N. Dubey[2], Tilman Schirmer[2], Florian P. Seebeck[1]*

[1] Department of Chemistry, University of Basel, Mattenstrasse 24a, Basel 4002, Switzerland

[2] Focal Area Structural Biology and Biophysics, Biozentrum, University of Basel, 4056 Basel, Switzerland

*To whom correspondence should be addressed: florian.seebeck@unibas.ch

ABSTRACT: Sulfoxide synthases are non-heme iron enzymes that catalyze oxidative carbon-sulfur bond formation between cysteine derivatives and N-α-trimethylhistidine as a key step in the biosynthesis of thiohistidines. The complex catalytic mechanism of this enzyme reaction has emerged as the controversial subject of several biochemical and computational studies. These studies all used the structure of the γ-glutamyl cysteine utilizing sulfoxide synthase, *Mth*EgtB from *Mycobacterium thermophilum* (EC 1.14.99.50), as a structural basis. To provide an alternative model system we have solved the crystal structure of *Cth*EgtB from *Chloracidobacterium thermophilum* (EC 1.14.99.51) that utilizes cysteine as a sulfur donor. This structure reveals a completely different configuration of active site residues that are involved in oxygen binding and activation. Furthermore, comparison of the two EgtB structures enables a classification of all ergothioneine biosynthetic EgtBs into five sub-types, each characterized by unique active-site features. This active site diversity provides an excellent platform to examine the catalytic mechanism of sulfoxide synthases by comparative enzymology, but also raises the question as to why so many different solutions to the same biosynthetic problem have emerged.

INTRODUCTION

EgtB is a non-heme iron-dependent sulfoxide synthase that participates in the biosynthesis of ergothioneine (**1**, Figure 1).[1-3] EgtB catalyses oxidative carbon–sulfur (C-S) bond formation between the imidazole ring of *N*-α-trimethyl histidine (TMH, **2**, Figure 1) and γ-glutamyl cysteine (γ-GC) or cysteine. [2, 4-9] Subsequent oxidation of the sulfur atom concludes the four-electron reduction of molecular oxygen (Figure 1) and produces a histidinyl-γ-GC sulfoxide conjugate (**3**, Figure 1) or the histidinyl-cysteine sulfoxide conjugate (**4**). Discovery of EgtB and other ergothioneine biosynthetic enzymes opened new avenues in deciphering the complex biological function of this sulfur compound. For example, studies on *Mycobacterium tuberculosis*, *Burkholderia thailandensis* and *Aspergillus fumigates* showed that deletion of ergothioneine biosynthetic genes reduces tolerance against oxidative stress, suggesting that ergothioneine plays an important role in the redox homeostasis in these pathogenic microorganisms.[7, 10-12]

From a chemical perspective, EgtB is of particular interest because this enzyme represents an entirely new catalyst type, distinguishable from any other oxygen-utilizing enzyme by its reactivity and structure. For example, unlike α-ketoglutarate-dependent oxygenases which adopt a jelly-roll fold,[3, 13] sulfoxide synthases adopt a two-domain structure containing a C-terminal domain related to the copper-dependent formylglycine generating enzyme (FGE-like domain)[14-15] and a N-terminal domain that is most homologous to zinc-dependent thiol-S transferases (DinB_2 domain).[16] The crystal structure of EgtB from *Mycobacterium thermoresistibile* (*Mth*EgtB) revealed that the active site is located at the interface between the two domains.[1, 17-18] The active site hosts a three-histidine facial triad as a metal binding motif, and several residues that are essential for TMH- and γ-GC-binding. Subsequent biochemical analysis implicated Tyr377 as an essential catalytic residue.[17, 19] Mutating Tyr377 to Phe resulted in an enzyme that produces γ-GC dioxide instead of sulfoxide **4**.[17] Analogous experiments with the ovothiol biosynthetic sulfoxide synthase OvoA showed that this distant relative of *Mth*EgtB uses an equivalent Tyr residue (Tyr417) in the same way.[19] Both studies concluded that an active site tyrosine plays a pivotal role in steering an early catalytic intermediate towards sulfoxide production and away from thiol dioxygenation. However, the mechanism by which Tyr377 or Tyr417 influence reactivity remains disputed.[17, 20-22]

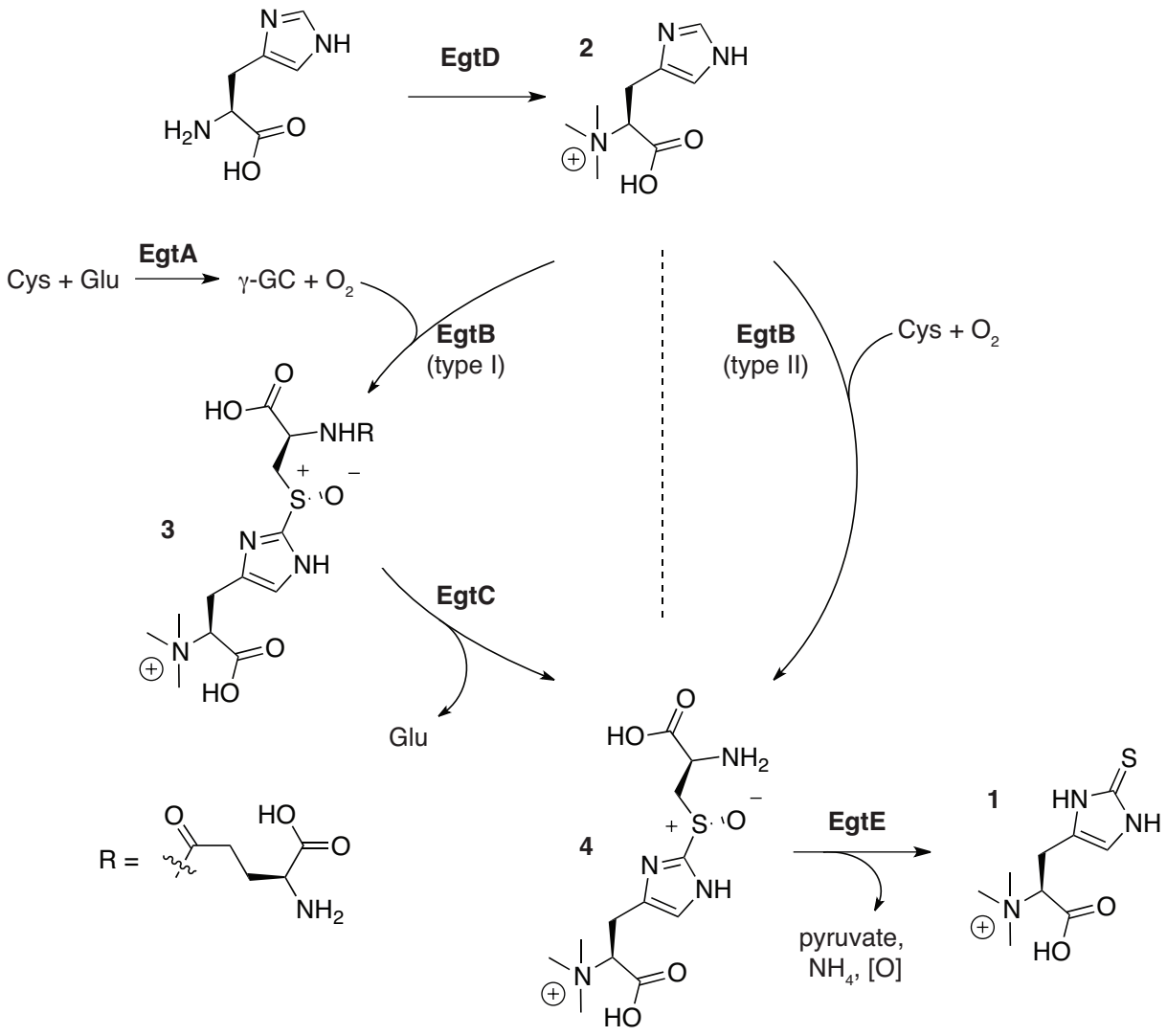

Figure 1: *Mycobacterial* ergothioneine (**1**) biosynthesis starts with histidine and is catalyzed by the enzymes EgtABCDE (left).[2] Thre key reaction, oxidative sulfurization of TMH (**2**) is catalyzed by a type I EgtB. Other bacteria, such as *Chloracidobacterium thermophilum* and most fungi utilize a cysteine specific type III or IV sulfoxide synthase, in a three-step pathway.[4-9]

Given the functional importance of Tyr377 we were surprised to find that a large sub-class of EgtB homologs lack this residue.[11] Most of these enzymes are encoded by Proteobacteria but also occur in several species from other phyla (SI Table 1). To understand how these EgtB homologs could support ergothioneine production, we examined the crystal structure and kinetic behavior of EgtB from *Chloracidobacterium thermophilum* (*Cth*EgtB). This study highlighted five important differences between *Mth*EgtB and *Cth*EgtB. First, *Cth*EgtB uses Cys instead of γ-GC as a sulfur donor; secondly, *Cth*EgtB utilizes a tyrosine from the N-terminal domain for the exact same function as Tyr377 in *Mth*EgtB; third, the *Cth*EgtB active site employs a second active site tyrosine; fourth, a large section of the rigid active site observed in *Mth*EgtB is replaced in *Cth*EgtB by two mobile active site loops that fold in a substrate-dependent fashion; finally, all *Cth*EgtB-type EgtBs appear to adopt a D_2-symmetric tetrameric quaternary

structure. Because of these structural differences to *Mth*EgtB, *Cth*EgtB provides a complementary study system that may help to solve the emerging controversy about the catalytic mechanism of sulfoxide synthases. Furthermore, comparison between the structures of *Mth*EgtB and *Cth*EgtB, compounded by phylogenetic analysis of other homologs illuminates the evolutionary origin of sulfoxide synthases and raises the question as to what evolutionary pressures may have given rise to the observed active site diversity within the enzyme class of sulfoxide synthases.

RESULTS

Crystal structure determination of *Cth*EgtB. The structure of *Cth*EgtB was determined by X-ray crystallography. *Cth*EgtB was crystallized as the native protein in complex with iron (II). The crystal diffracted to a resolution of 2.0 Å and belonged to space group $P2_1$ with four monomers in the asymmetric unit. For data collection and refinement statistics, see Tables S2 and S3, respectively. The crystal structure was solved by molecular replacement using a homology model built from the native structure of *Mth*EgtB (PDB: 4X8E) as a search model. *Mth*EgtB and *Cth*EgtB share 32 % sequence identity. The electron density revealed a continuous polypeptide chain from residues 17 to 434 with the exception of segments 93-98, 183-193, and 377-384 (Figure S1). In presence of TMH, *Cth*EgtB was crystallized in space group $C222_1$ with cell constants a, c = 108 Å, b = 200 Å. *Cth*EgtB crystals containing TMH were obtained through co-crystallization. The structure of the *Cth*EgtB/Fe/TMH complex was solved to 2.2 Å by molecular replacement with the native *Cth*EgtB model. The (2Fo-Fc) electron density map showed well-defined density into which two of the previously missing regions (loop 1: residues 93-98 and loop 2: 378-384) could be fitted resulting in a model comprising all residues from 7 to 434 aside from residues 183-193 of the linker between the N- and C-terminal domain (Figure 2A, Figure S2). The TMH ligand could be unambiguously modeled into the (Fo-Fc) difference density map (Figure S3). Data collection and refinement statistics are summarized in the supporting information as Table 2 and Table 3, respectively.

***Cth*EgtB forms a stable tetramer.** Overall, the tertiary structure of *Cth*EgtB (Fig. 2A) is strikingly similar to that of *Mth*EgtB (Fig. S4; r.s.m.d. = 1.2 Å for 1709 of 2341 aligned), despite the moderate sequence. The most important differences between the two homologs are their quaternary structures and the organization of the active sites. In the native *Cth*EgtB crystals, the four molecules of the asymmetric unit form a tetramer of D2 symmetry, assembled *via* two interfaces, each with a two-fold axis (Figure 2B). The same tetramer is observed in the *Cth*EgtB/TMH crystal, but with one of the molecular dyads coincident with a crystallographic 2-fold axis (running along the C-terminal interface). Also in solution, as evidenced by size exclusion chromatography, *Cth*EgtB forms a tetramer, in contrast to monomeric *Mth*EgtB [1] (Fig. S5). The N-terminal interface (Fig. 2D) occurs between ends of the α-helix bundle N-terminal domain with an interface area of 1310 $Å^2$. Two salt bridges are formed by Arg111 and Asp44, while the following residue pairs form hydrogen bonds: Val114 (backbone) and Glu43, Arg111 and Asp44, Thr110 and Asp444, Thr171 and Leu108 and Asn172 and Arg111 (backbone). The C-terminal interface (Fig. 2C). spans a slightly

smaller area (1094 Å^2), and the interacting residues are fewer in number and less conserved. Arg376 and Asp 432 form a salt bridge while the residue pairs Ser260 and Lys 388, Tyr308 and Asn392, and two symmetry-related Asn392 residues form hydrogen bonds. Residues Thr/Ser110, Arg111, Asn172, Glu43 are conserved in all type II EgtBs (see discussion) suggesting that in general type II EgtB might be tetrameric.

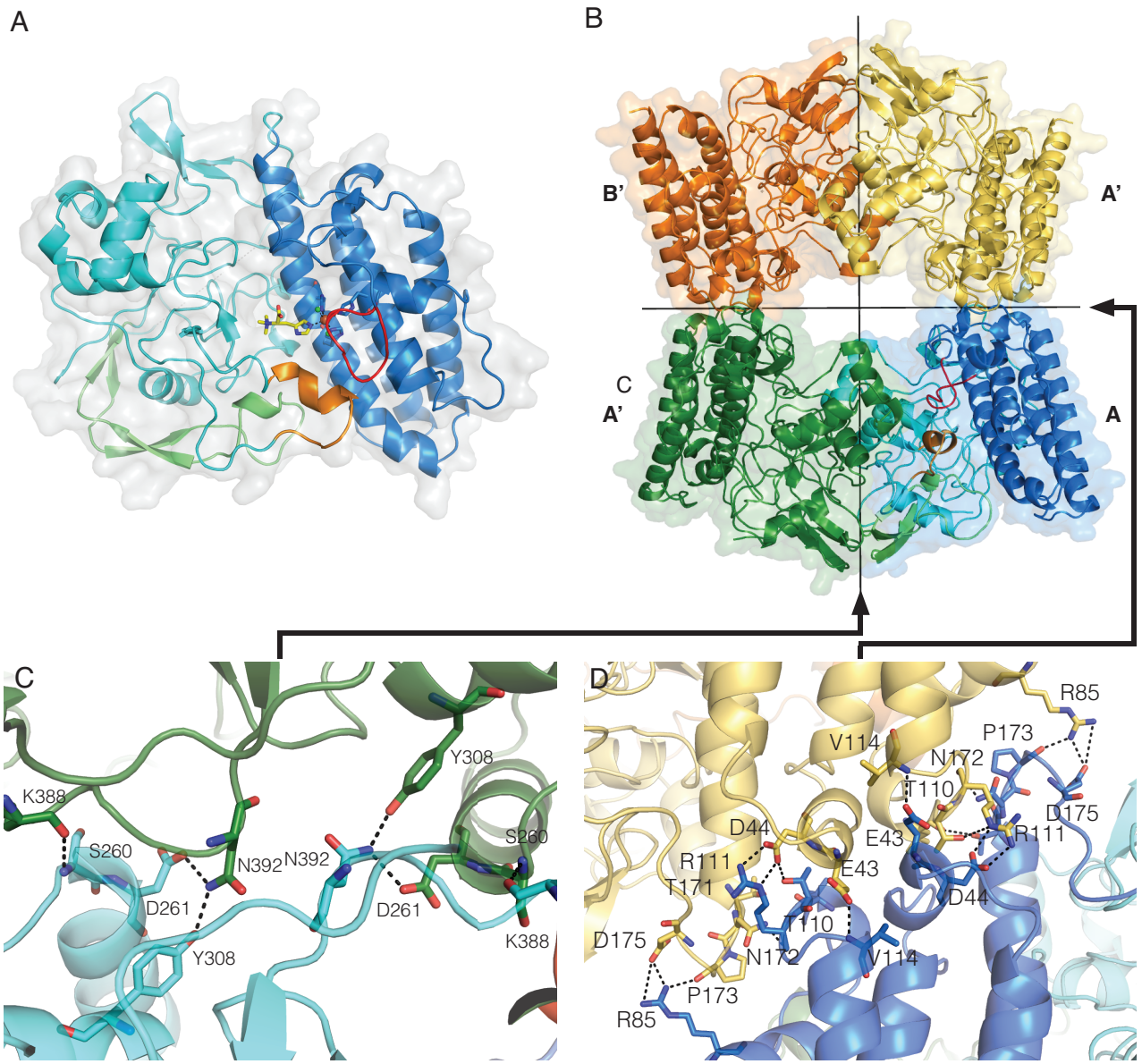

Figure 2: Structural and Oligomeric Analysis of *Cth*EgtB in complex with TMH A: Cartoon of the monomeric ***Cth*EgtB**/Fe/TMH structure. The N-terminal DinB_2-like domain (residues 17-176) is show in dark blue while the C-terminal FGE-like domain is shown in green (residues 198-234) and light blue (residues 235-434). Active site loop 1 (93-99) in red, and active site loop 2 (378-386) in orange, close over the active site. The substrate TMH (yellow), iron (orange), chloride ligands (green), iron (brown), and the metal coordinating histidines (blue) are shown to indicate the location of the active site. **B:** View of the tetrameric structure, with two of the three 2-fold axes shown indicating the two different interfaces, the N-terminal & C-terminal interface. The third dyad is perpendicular to the page. C, D: Close-up views onto the C-terminal (C) and N-terminal (D) interfaces with interacting residues shown in full. Dashed lines indicate H-bonds.

Active site of *Cth*EgtB. The structure of *Cth*EgtB in complex with TMH shows that the imidazole rings of His62, His153 and His157 form an iron-binding three histidine facial triad, with the Nτ of the TMH imidazole ring joining as the fourth. The Nπ of this imidazole ring hydrogen bonds with the backbone carbonyl 385 via a bridging water molecule (Figure 3A). In the native structure loop 2 containing Tyr385 is unresolved, suggesting that the presence of TMH immobilizes this loop. The N-α-trimethylamino moiety of TMH is boxed in by the aromatic rings of Phe415 and Phe416. Furthermore, each of the three N-methyl groups also interact with the carbonyl groups of either Phe415 (3.2 Å, backbone), Gln156 (3.2 Å, side chain) or Asn414 (3.4 Å, side chain). Comparison to *Mth*EgtB shows that both sulfoxide synthases recognize TMH by an analogous set of interactions (Figure 3A & E).

The remaining two coordination sites in the *Cth*EgtB/TMH complex are occupied by residual electron density that is best modeled by two chloride ligands: the axial chloride, binding opposite to His156 (Cl_{ax}), and the equatorial chloride, binding opposite to His152 (Cl_{eq}). Modelling the two features as water molecules did not sufficiently reduce the residual electron density. While the modelled Fe-Cl distances are slightly longer than expected for Fe-Cl bonds (Fe-Cl_{ax}, Fe-Cl_{eq}: 2.5 Å), it has also been noted that hydrogen bonding interactions to Cl may be involved in lengthening the Fe–Cl bond.[23-24] During catalysis one of these two sites must coordinate the second substrate cysteine. However, for reasons that may be related to the flexibility of loop 1 and 2 we were unable to obtain crystals of *CthEgtB* with bound cysteine despite an extensive search for appropriate crystallization and soaking conditions. As an alternative, we modelled the *Cth*EgtB/TMH/Cys complex (Figure 3C) using the structure of *Mth*EgtB in complex with manganese (II), *N*-α-trimethyl histidine (DMH) and γ-GC as a template (Figure 3E). In *Mth*EgtB the sulfur atom of γ-GC occupies the axial coordination site (Figure 3E). The cysteinyl carboxylate interacts with Arg87 and Arg90 and the glutamyl moiety salt bridges with Asp416 and Arg420. Finally, the amide function of γ-GC hydrogen bonds with the carboxylate of TMH. The model of the *Cth*EgtB/TMH/Cys complex shows that most of these interactions are conserved. The cysteine carboxylate makes a similar interaction with Arg103 and Arg106, and the α-amino group interacts with the carboxylate of TMH (Figure 3C). As a key difference, the *Mth*EgtB residues that are responsible for binding the glutamyl moiety of γ-GC, are replaced by Phe416 and Ala420 in *Cth*EgtB. These two mutations provide a clear structural explanation for the distinct substrate specificity among type I and II EgtBs.

The most intriguing structural differences between *Mth*EgtB and *Cth*EgtB map to the presumed oxygen binding site, which is occupied by Cl_{eq} in the *Cth*EgtB/TMH complex (Figure 3B).[1, 20-22] The side chain hydroxyl-groups of Ser92, Tyr93, and Tyr94 of loop 1 point towards the presumed oxygen binding site. The β-hydroxyl side chain of Ser92 was resolved in two conformations in which the β-hydroxyl side chain hydrogen bonds either with the axial or the equatorial chloride ligands (O-Cl_{ax}: 2.9 Å, and O-Cl_{eq}:

3.1 Å) (Figure 3D). The hydroxyl group of Tyr93 makes no direct contact with Cl_{eq} (Cl_{eq}-O: 4.0 Å), but instead hydrogen bonds to the backbone carbonyl of Tyr385 (2.9 Å), and packs against the imidazole ring of TMH (O-C_2: 3.1 Å). The aromatic ring of Tyr94 makes π–π stacking interaction with Tyr93, and the hydroxyl group of Tyr94 is juxtaposed with the Cl_{eq} (Cl_{eq}-O: 3.4 Å). Although this is a long distance for efficient hydrogen bonding, we note that the Tyr94 hydroxyl group is embedded in a largely hydrophobic environment formed by Phe66, Leu382 and Tyr385 providing no alternative hydrogen bonding partners. Hence, slight structural adjustments in the reactive complex would allow strong interactions between Tyr94 and iron-bound oxygen.

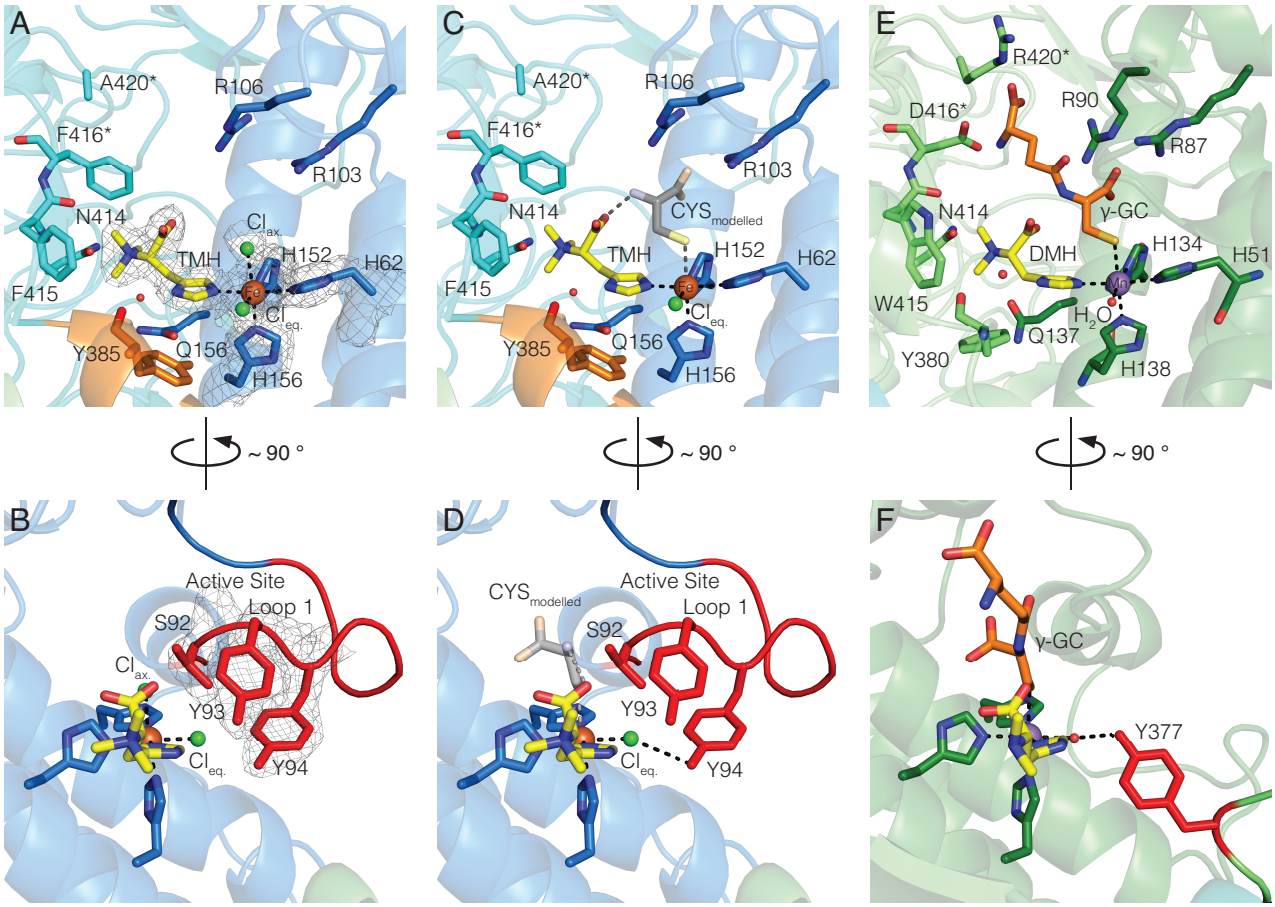

Figure 3. Structural Comparison of the active site of *Cth*EgtB with *Mth*EgtB. Important metal or substrate binding residues are shown as sticks and are colored according domain or segment. Fe is shown in brown, Mn in purple, DMH in yellow, modelled CYS in gray, γ-GC in orange, Cl ions and water as spheres in green and red respectively. **Upper Panel:** A front on view of the active site, focusing on the metal co-ordination sphere and TMH and γ-GC/Cys binding sites. Active site loop 1 has been omitted for clarity. **Lower panel:** This view focuses on the oxygen binding site and is rotated by approximately 90 °to the left from the front view. Active site loop 2 has been omitted for clarity. **A & B:** Active site of *Cth*EgtB in complex with iron (II), and TMH. The 2m|Fo|-D|Fc| omit map for iron, the three histidine ligands, TMH, S92, Y93 & Y94 (red) and the axial (Cl_{ax}) and equatorial chloride (Cl_{eq}) is contoured at σ-level = 1 . **C** & **D:** Cysteine is modelled into to the active site of *Cth*EgtB based on the location of the cysteinyl moiety of γ-GC in *Mth*EgtB. Proposed interactions are shown by dashed lines. **E** & **F:** Active site of *Mth*EgtB (4X8D) with Y377 pointing towards the proposed oxygen binding site occupied by a water molecule (red sphere).

The apparent active site geometry of *Cth*EgtB raises two important propositions. Firstly, the presence of Tyr93 and Tyr94 close to the presumed oxygen-binding site is highly suggestive of a catalytic role for one or both of these residues. This is interesting because the oxygen-binding pocket of *Mth*EgtB contains only one tyrosine (Tyr377). Superposition of the *Mth*EgtB with *Cth*EgtB structures shows that the phenol function of Tyr377 is positioned roughly between the phenol functions of Tyr93 and Tyr94 (Figure 4A). Therefore, based on structural comparisons alone it is impossible to decide which of the two Tyr residues in *Cth*EgtB could assume the same catalytic role as Tyr377 in *Mth*EgtB. Secondly, comparison of the *Cth*EgtB native structure and that of the *Cth*EgtB/TMH complex show that TMH-induced loop-folding converts a wide-open crevice to a tightly closed pocket. In the closed structure the presumed oxygen-binding pocket is completely engulfed by the metal center, the substrates and the side chains of Ser92, Tyr93 and Tyr94, suggesting that efficient oxygen-binding may require unfolding of loop 2. Hence, the two *Cth*EgtB structures provide evidence that loops 1 and 2 are flexible, and that their folding and unfolding may be obligatory steps in each catalytic cycle to allow substrate binding and product release. In *Mth*EgtB oxygen binds to the equivalent equatorial coordination site,[1, 20-22] but the shape of this pocket is different. This pocket is connected to the protein exterior by a narrow water-filled tunnel. Crystal structures of *Mth*EgtB in native form and in complex with TMH or with TMH and γ-GC show that this tunnel does not change shape upon substrate binding, suggesting that oxygen uptake does not require large-scale conformational change.[1]

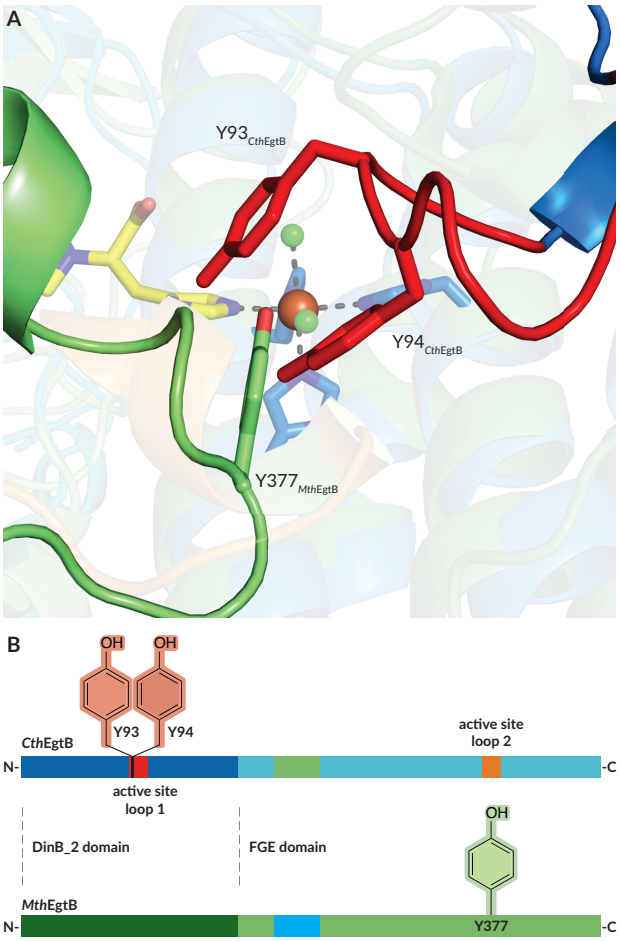

Figure 4. Comparison of the catalytic residues of *Cth*EgtB and *Mth*EgtB A): Superposition of the *Mth*EgtB (green) and *Cth*EgtB (red) active sites. The iron coordination sphere of Fe in the CthEgtB is shown faintly in the background. Tyrosine residues from *Mth*EgtB (green) and *Cth*EgtB (red) with an assigned catalytic function are shown in full. **B):** Schematic representation of the architecture of *Mth*EgtB & *Cth*EgtB.

Table 1[a]

Enzyme	$k_{cat,cys}$[b] [s^{-1}]	$K_{M,cysteine}$ [10^{-6} x M^{-1}]	$k_{cat,4}$[c] [s^{-1}]	$K_{M,TMH}$ [10^{-6} x M^{-1}]	$k_{cat,cys}/k_{cat,4}$
*Cth*EgtB$_{wt}$	0.14 ± 0.05	27 ± 3	0.2 ± 0.01	65 ± 2	1
*Cth*EgtB$_{Y93F}$	0.16 ± 0.03	120 ± 30	0.0004 ± 0.0001	5 ± 1	400
*Cth*EgtB$_{Y94F}$	0.021 ± 0.004	34 ± 12	0.003 ± 0.001	35 ± 10	7
*Cth*EgtB$_{Y93F, Y94F}$	0.049 ± 0.003	90 ± 15	< 0.0001	n.d.[d]	> 500

[a]Kinetic parameters were determined in the presence of 4 uM $FeSO_4$, 2 mM TCEP, 2 mM ascorbate, 100 mM NaCl, 100 mM HEPES, pH 8.0 at 26 °C. Rate determined by monitoring the consumption of cysteine[b], or the production of sulfoxide **4**[c]. [d] n.d. = not determined.

Catalytic activity of *Cth*EgtB and variants thereof. We characterized the catalytic activity of *Cth*EgtB using the same HPLC-based kinetic assay as previously developed for *Mth*EgtB (Table 1).[1, 17] In brief, reactions containing TMH, cysteine, iron sulfate, tris(2-carboxyethyl)phosphine (TCEP) and ascorbate were initiated by addition of purified *Cth*EgtB. Reaction products were analyzed by ^{1}H NMR and RP-HPLC. An initial experiment showed that *Cth*EgtB accepts cysteine to make sulfoxide **4** (Figure 1) but cannot turnover γ-GC. By monitoring time-dependent production of **4** we determined k_{cat} for sulfoxide production ($k_{cat,4}$) and K_M for TMH ($K_{M,TMH}$) in the presence of 0.5 mM cysteine (Figure S8a). We also monitored the consumption of cysteine to determine $k_{cat,cys}$ and K_M for cysteine ($K_{M,cys}$) in the presence of 0.2 mM TMH (Figure S8b). ^{1}H NMR analysis of reactions that initially contained 1 mM TMH and 0.5 mM cysteine showed that wild type *Cth*EgtB oxidizes about 20 % of cysteine to cysteine sulfinic acid, and 80 % to sulfoxide **4** (Figure S5 & S6). The same side reactivity has been reported for EgtB from *Burkholderia thailandensis*,[11] and OvoA from *Erwinia tasmaniensis*.[19, 25] Mechanistic investigations on *Mth*EgtB and on OvoA from *Erwinia tasmaniensis* showed that this side activity occurs because an early reaction intermediate can react either to form the sulfoxide or to form thiol dioxide.[17, 19]

To probe the catalytic contributions of Tyr93 and Tyr94 we mutated either, or both residues to Phe. ^{1}H NMR analysis of reaction mixtures showed that *Cth*EgtB$_{Y93F}$ and *Cth*EgtB$_{Y94F}$ both produced cysteine sulfinic acid as the main product, and almost no sulfoxide **4** (Figure S10 & S11). Subsequent determination of the Michaelis-Menten parameters showed that the Tyr93Phe mutation slightly increased the apparent K_M for cysteine and reduced the apparent K_M for TMH by ten-fold (Table 1). The phenol function of Tyr93 makes direct contact with C_2 of the TMH imidazole ring (3.1 Å). This interaction may be unfavorable and hence deletion of the hydroxyl group in *Cth*EgtB$_{Y93F}$ could stabilize the enzyme/substrate complex. Alternatively it is possible that $K_{M,TMH}$ is lowered due to a kinetic effect. Because the mutation reduced k_{cat} (see below) relative to the rates of binding and unbinding of TMH the value of $K_{M,TMH}$ could approach than of a true binding constant ($K_{D,TMH}$). Mutation of Tyr94 reduced $K_{M,TMH}$ only by two-fold, and caused no significant effect on $K_{M,Cys}$. Hence, the observed reduction of sulfoxide synthase activity is not due to defects in cysteine- or TMH-binding.

On the other hand, the turnover rates ($k_{cat,4}$) for sulfoxide production were strongly affected in all variants. Mutating Tyr93 reduced $k_{cat,4}$ by 500-fold, but left the rate of cysteine consumption ($k_{cat,cys}$) essentially unchanged. As evidenced by the NMR analysis discussed above, *Cth*EgtB$_{Y93F}$ produces almost exclusively cysteine sulfinic acid, instead of sulfoxide **4**. Mutating Tyr94 reduced sulfoxide synthesis by 70-fold and cysteine consumption by 7-fold. The double mutant showed no detectable sulfoxide production, and a cysteine consumption activity only 3-fold less than that of wild type. Summarizing these results we arrive at the following conclusions: a) the phenol functions of both active site tyrosines are important for catalysis but are unimportant for substrate

binding; b) Tyr93 is more important in determining the product specificity than Tyr94, c) Tyr93 is entirely dispensable for oxidative cysteine consumption, d) Tyr94 plays a significant role in oxidative cysteine consumption, e) in the absence of Tyr93, Tyr94 supports sulfoxide production at a low but observable rate.

Further evidence that both tyrosines are involved in catalyzing sulfoxide production comes from the fact that both mutations induce a significant solvent kinetic isotope effect (sKIE). Measuring sulfoxide production rates in the presence of saturating substrate concentrations in either H_2O or D_2O revealed a sKIE of 1.3 ± 0.2 for the wild type, 2.8 ± 0.2 for *Cth*EgtB$_{Y93F}$ and 3.9 ± 0.2 for *Cth*EgtB$_{Y94F}$ (Figure S12) The effects of the Tyr93Phe mutation in catalysis is very similar to those observed for the mutation of Tyr377 in *Mth*EgtB, and Tyr417 in OvoA.[17, 19] In both cases elimination of this catalytic acid reduced sulfoxide synthase activity dramatically, induced a significant sKIE, but did not affect the ability to use oxygen and oxidize thiols. However, the presence and catalytic importance of a second tyrosine in *Cth*EgtB*B* has no correspondence in previously characterized sulfoxide synthases.

DISCUSSION

*Cth*EgtB and *MthEgtB* catalyze almost identical reactions. Therefore, the structural differences between the two active sites are both surprising and informative. The current proposals explaining the catalytic mechanism of sulfoxide synthases were all developed based on the structure of *Mth*EgtB. As discussed below, reevaluation of these proposals in view of the structure of *Cth*EgtB provides a new test that may help to distinguish between different models. In the second part of the discussion we introduce a classification of all known ergothioneine biosynthesis sulfoxide synthase into five types, and we propose a possible evolutionary trajectory by which this diversity among extant sulfoxide synthases may have emerged.

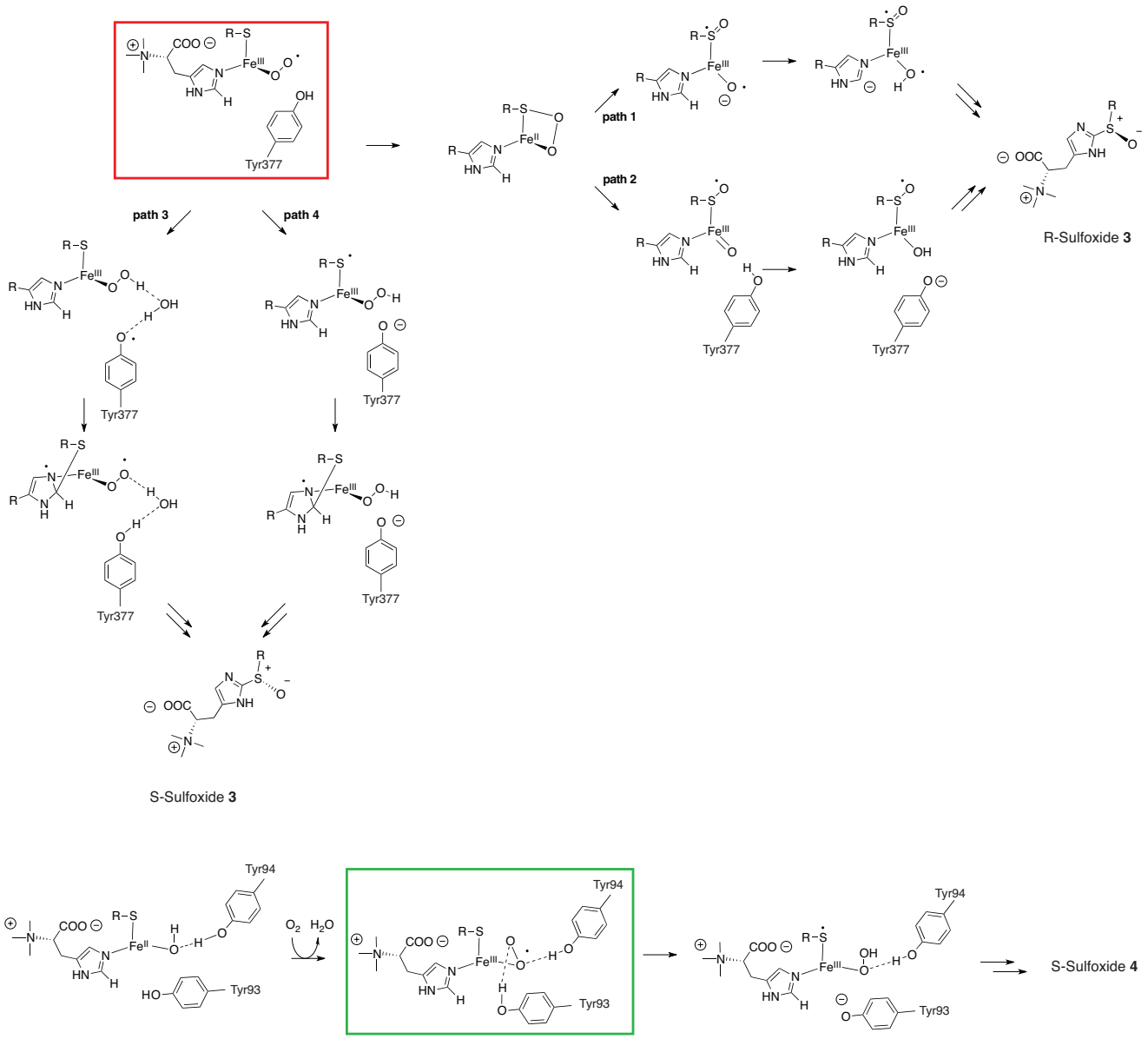

Figure 5. Top: Catalytic mechanisms proposed for *Mth*EgtB, adapted from Ref. 1, 20 – 22. Two computational studies propose that the reactive enzyme/substrate complex (*Mth*EgtB/Fe/TMH/γ-CG/O_2 complex, red box) first reacts via oxygen atom transfer to the sulfur atom of γ-GC (**paths 1** & **2**). Both models predict the formation of sulfoxide **3** with R-configuration at the sulfur atom. [21-22] Two alternative models suggest that the reactive complex first reacts via reduction of the superoxide ligand, followed by C-S bond formation between TMH and γ-GC (**paths 3** & **4**). This trajectory leads to formation of the sulfoxide **3** with S-configuration.[1, 20] **Bottom**: proposed roles of Tyr93 and 94 in the reactive complex of *Cth*EgtB (*Cth*EgtB /Fe/TMHCys/O_2 complex, green box, see text).

***Mth*EgtB-based proposals for the catalytic mechanism of sulfoxide synthases**. The four main proposals for the mechanism of *Mth*EgtB catalyzed C-S bond formation (paths 1 – 4, Figure 5) all assume that the enzyme combines with the substrates TMH, γ-GC and oxygen to form an iron (III) superoxide complex as a first intermediate (red box, Figure 5).[1, 20-22] Even though enzyme-

bound iron (III) superoxides are notoriously difficult to detect, growing evidence suggests that these species form as early intermediates in many non-heme iron enzymes.[26-31] The disagreement among the four models starts with the next step. Two computational studies concluded that oxygen transfer to the sulfur atom of γ-GC occurs first (paths 1 & 2, Figure 5).[21-22] Both models suggest that Tyr377 serves as a proton donor to the iron coordinated oxygen atom (proximal oxygen), after cleavage of the O-O bond. Subsequent C-S bond formation between γ-GC and TMH produces a sulfoxide with R-configuration (R-sulfoxide **3**). This prediction is the weakest aspect of these models because the enzymatic product has been determined to be the S-sulfoxide **3**.[32] The remaining two models, one based on structural and biochemical analysis (path 4), the other based on QM/MM calculations (path 3) favor a reaction path where the iron (III) superoxide is first reduced by accepting a proton and an electron. In these models C-S bond formation precedes S-O bond formation which leads to the correct sulfoxide stereochemistry. The two models disagree over the specific role of Tyr377. The computational analysis identified a low-energy pathway along which the iron (III) superoxide is reduced by hydrogen atom transfer from Tyr377 (path 3, Figure 5). However, the calculations also showed that the radical character transfers from Tyr377 to the sulfur atom of γ-GC en route to the transition state of the C-S bond forming step. Hence, it remains an open question as to whether oxidation of Tyr377 represents a necessary – on the pathway – step, or whether γ-GC and Tyr377 share radical character in an equilibrium prior to C-S bond formation. An important feature of this computational model is that in the reactive complex Tyr377 retracts form the position observed in the crystal structure and only interacts with the iron:oxygen species via an intervening water molecule (Figure 5, path 3). There is no empirical evidence for such a movement. In fact, the active site geometry of *Mth*EgtB, and specifically the position of Tyr377 were found invariant among different complexes of *Mth*EgtB.[1] The last model (path 4, Figure 5) suggests that the iron (III) superoxide is reduced by proton transfer from Tyr377 and electron transfer from the iron-coordinated γ-GC.[17] In this way γ-GC is directly activated as a radical that can attack the imidazole ring of TMH.

Importantly, the four models assign different functions to Tyr377 in the early reaction stage, depending on whether its phenol ring interacts with the proximal or the distal oxygen of the iron (II) superoxide species, or whether there is no direct interaction at all. The position of Tyr377 as determined by crystallography does not allow a distinction between these models. As discussed below *Cth*EgtB provides a related system featuring a tyrosine (Tyr93) residue with the same catalytic functions as Tyr377 that cannot interact with the proximal oxygen atom.

Catalytic roles of Tyr93 and Tyr94 in *Cth*EgtB. Our Structural and kinetic observations implicate Tyr93 and Tyr94 as important catalytic residues. The phenotypes of the Tyr93Phe mutation – i) dramatic reduction of sulfoxide synthase activity, ii) retainment of cysteine oxidation activity, and iii) introduction of a significant sKIE on the residual sulfoxide synthase activity – match the phenotypes induced by the Tyr377 mutation in *Mth*EgtB, and the Tyr417 mutation in OvoA.[17, 19] This evidence supports the con-

clusion that Tyr93 serves the same catalytic function as Tyr377 and Tyr417 despite their different location in the primary sequence, and the different orientation in the active site (Figure 3C & D).

The second tyrosine in the oxygen binding pocket of *Cth*EgtB, Tyr94, introduces a new aspect to the catalytic mechanism of sulfoxide synthases. Tyr94 is juxtaposed to the coordination site that is either occupied by water, oxygen or, as seen in the crystal structure, by Cl_{eq} (Figure 3D). This position strongly implicates Tyr94 as a hydrogen bonding partner to iron (II)-bound water or to the proximal oxygen of iron (III)-bound superoxide (green box, Figure 5). This interaction is likely strong, because Tyr94 has no apparent alternative hydrogen bonding partner. Mutation of this residue affected sulfoxide production by 70-fold, but also reduced oxidative cysteine consumption by 7-fold, suggesting that Tyr94 assists the catalytic cycle in two independent steps. First, Tyr94 plays a supporting role in guiding the iron (III) superoxide towards the sulfoxide production pathway. One way how Tyr94 could do so is by hydrogen bonding with the proximal oxygen of the iron (III) superoxide species (Figure 5). This acidic interaction would certainly increase the electron affinity of the iron (III) superoxide species and thereby facilitate its reduction in the first catalytic step. The observation of a sizable sKIEs in the Tyr94Phe mutant is consistent with this interpretation: this mutation could make the iron (III) superoxide species less oxidative, rendering proton-coupled electron transfer to this species rate limiting. An alternative interpretation of the *Cth*EgtB$_{Y94F}$ phenotype would be that Typ94 acts as a hydrogen bond donor to Tyr93 to activate the later as a catalytic acid. However, in the crystal structure the two phenol groups of Tyr93 and Tyr94 are separated by 4 Å, and in the conformation given, do not possess a geometry that could facilitate hydrogen bonding. Direct hydrogen bond between the two residues might be weak at best.

Reduced cysteine consumption activity in *Cth*EgtB$_{Y94F}$ indicates that Tyr94 is also involved in oxygen binding and activation. The Tyr94Phe mutation could affect this activity in two ways: the lack of a proton donor could slow down protonation and removal of the iron (II) coordinated hydroxide and thereby slow down oxygen binding (bottom, Figure 5). Alternatively, the lack of a hydrogen bond could destabilize the iron (III) superoxide. A similar interaction has been observed in human and murine cysteine dioxygenase (CDO, EC 1.13.11.20).[33] Although CDOs are entirely unrelated to sulfoxide synthases, the local geometries around the catalytic iron center are remarkably similar.[17] CDO also coordinate iron (II) by three-his facial triads. In the reactive complex the remaining coordination sites are filled by amine- and thiolate-ligands form the substrate cysteine. Finally, addition of oxygen as the last ligand gives rise to an iron (III) superoxide. CDO also contains a second-coordination sphere tyrosine (Tyr157) that hydrogen bonds with the iron-coordinated oxygen.[34-35] Mutation of Tyr157 to Phe resulted in 8 - 20-fold reduction of dioxygenase activity, showing that Tyr157 – similar to Tyr94 in *Cth*EgtB – is important but not crucial for the oxygen activation by CDO.[33, 36] The double mutant *Cth*EgtB$_{Y93F, Y94F}$ lacks any measurable sulfoxide synthase activity, and oxidizes cysteine 3-fold less efficiently than wild type or *Cth*EgtB$_{Y93F}$ (Table 1). This activity pattern shows that the Tyr93Phe and Tyr94Phe mutations lead to additive

effects, and that the two Tyr residues have limited capacity to compensate for the absence of each other. Hence the two tyrosines must play complementary roles that are related to their specific position relative to the oxygen binding site.

A tyrosine residue near the oxygen binding site of non-heme iron enzyme automatically raise the question as to whether this residue participates in the redox chemistry. Oxygen can react with ferrous iron to produce highly reactive species that could oxidize the comparatively electron-rich tyrosine side chain. Oxidation of active site residues could either be part of the catalytic mechanism, or could lead to maturing or deactivating automodifications.[37] The endoperoxide forming enzyme FtmOx1 provides an example of redox active tyrosine involved in the catalytic mechanism.[38] In the taurine dioxygenase TauD, oxidation of active site Tyr73 also occurs but is part of a deactivating side reaction.[39] In mammalian CDO the active site Tyr157 is cross-linked with a nearby Cys residue (Cys93) as a result of an oxygen-dependent side reaction.[40] Since mutation to Phe conserves most of the CDO activity, Tyr157 is unlikely to participate as an essential redox partner during cysteine deoxygenation. On the other hand, there are also enzymes that use tyrosine side chains to activate and orient iron-bound oxygen species with no apparent redox participation. A computational study on the algal prolyl-4-hydroxylase concluded that the active site tyrosine (Tyr140) controls the reactivity of the oxo-ferryl species by hydrogen bonding to the iron bound oxygen atom.[41] How Tyr140 evades oxidation remains an open question. The same is true for the sulfoxide synthases *Mth*EgtB and *Cth*EgtB. Even though Tyr377 and Tyr93/Tyr94 appear intimately involved with oxygen binding and activation, we have no evidence that these residues participate in any redox activity, and it is not yet clear why they do not.

In summary, the structural and kinetic evidence discussed above is consistent with the following interpretation: Catalysis by *Cth*EgtB requires two hydrogen bond donors in the oxygen binding site. Tyr94 hydrogen bonds with the proximal oxygen of the iron (III) superoxide complex to render this species more oxidative. Tyr93 transfers a proton to the distal oxygen of the iron (III) superoxide. This transfer is coupled to electron transfer from the substrate cysteine to form an iron (III) hydroperoxide and a thiyl radical (Figure 5). The relative positions of Tyr93 and Tyr94 compounded by their specific functions provide evidence that proton transfer occurs to the distal and not to the proximal oxygen. Analogous conclusions based on *MthEgtB* would be more ambiguous because in the available crystal structures Tyr377 adopts a position that allows interaction with either atom of the iron-coordinated superoxide (Figure 4). From this point forth, the main tenets of any mechanistic proposal will have to be consistent with the structures of both sulfoxide synthase types (*Mth*Egt*B* and *Cth*EgtB). We believe that this test will be of significant help in the elimination or validation of mechanistic proposals for the sulfoxide synthase catalyzed reaction.

The emergence of sulfoxide synthase diversity. The differences in the active sites of *Cth*EgtB and *MthEgtB* are also interesting from an evolutionary perspective. Apparently, the family of sulfoxide synthases does not comply with the general expectation that

essential catalytic residues and active site geometries are conserved among enzymes with similar functions.[42] Residues Tyr377 and Tyr93 map to completely different locations within the protein scaffold (Figure 4B), despite their identical roles in catalysis. Relocation of catalytic residues in enzymes with identical function has been documented both in natural and laboratory protein evolution. [42-48] The importance of spatial conservation – rather than conservation in the primary sequence – for catalysis has been noted. *Functional residue hopping* is typically facilitated by conservation of the rest of the active site. By contrast, the migration of a catalytic tyrosine in *Cth*EgtB (Tyr93) with respect to *Mth*EgtB (Tyr377) is accompanied by the introduction of a second catalytic tyrosine (Tyr94), change of substrate specificity, and conversion of a stiff active site (as in *Mth*EgtB) to an open active site covered by two flexibles. This complete remodeling raises the question as to what evolutionary path could lie between the two catalyst types, and what evolutionary pressure may have caused the conversion from one to the other type.

To address this question and to probe the evolutionary relationships of sulfoxide synthases, we constructed a phylogenetic tree based on seven EgtB homologs with characterized activities (Figure 6A).[1, 6-8, 17 9] Also, we inspected the alignment of the respective sequences for the absence or presence of motifs that are important for function in *Mth*EgtB or *Cth*EgtB (Figure 6B). Based on this analysis we distinguished five types of ergothioneine biosynthetic sulfoxide synthase (types I –V). Type I sulfoxide synthases utilize γGC, and type II – IV use cysteine as sulfur donor.[4-9, 11] Most type IV sulfoxide synthases are OvoA-like enzymes that use histidine and cysteine to produce a sulfoxide intermediate in ovothiol biosynthesis.[18] However, in the presence of TMH OvoA from *E. tasmaniensis* was shown to produce sulfoxide **3,** highlighting the functional similarity of between EgtBs and OvoAs.[49] Indeed, the OvoA homologs from *Microcystis aeruginosa* and other cyanobacteria have evolved to make sulfoxide **3** as their main physiological product. Hence, we included this cyanobacterial enzyme as representative of type VI ergothioneine biosynthetic sulfoxide synthase.[8] Finally, we also included the cyanobacterial EgtB from *Thermosynechococcus elongatus* as a representative of type V sulfoxide synthases. This type has not been fully characterized yet. Despite significant similarity to type I enzymes, the type V EgtBs accept neither cysteine nor γ-GC as substrate (Stampfli & Seebeck, unpublished).

Comparing these five enzyme types we arrived at the following conclusions (Figure 6): i) the motifs for iron and TMH binding are conserved in all types, ii) tyrosines equivalent to Tyr377 in *Mth*EgtB are conserved except in type II; iii) the γ-GC-recognition motif DXXR motif is exclusive to type I; iv) the RXXR motif that is responsible for γ-GC-binding in *Mth*EgtB, and for cysteine-binding in *Cth*EgtB occur in type I, II, and with slight variation (KXXR) in type V. In contrast, type III and type IV sulfoxide synthases lack this motif, suggesting that these enzymes bind cysteine in a completely different mode. Since most types use a Tyr377-like catalytic acid and are monomeric enzymes, we conclude that an ancestral sulfoxide synthase most likely shared these properties. Type II-IV use cysteine as sulfur donor, arguing that the ancestral enzyme too used this very common sulfur

metabolite. But why is the cysteine-binding pocket not conserved among the three types? Why should an ancestral enzyme undergo dramatic active site remodeling to arrive at a functionally equivalent solution? A more likely explanation for the emergence of thee enzymes with different substrate binding pockets would be that the ancestral sulfoxide synthase used a different sulfur donor than cysteine. Possible candidates could be hydrogen sulfite, thiosulfate or thiophosphate. This scenario suggests that this ancestral enzyme type (type 0) first entered different bacterial and fungal lineages and then adapted independently to utilize cysteine or γ-GC for ergothioneine biosynthesis. Consequently, there may not be an evolutionary path directly connecting extant (type I - V) sulfoxide synthases.

A

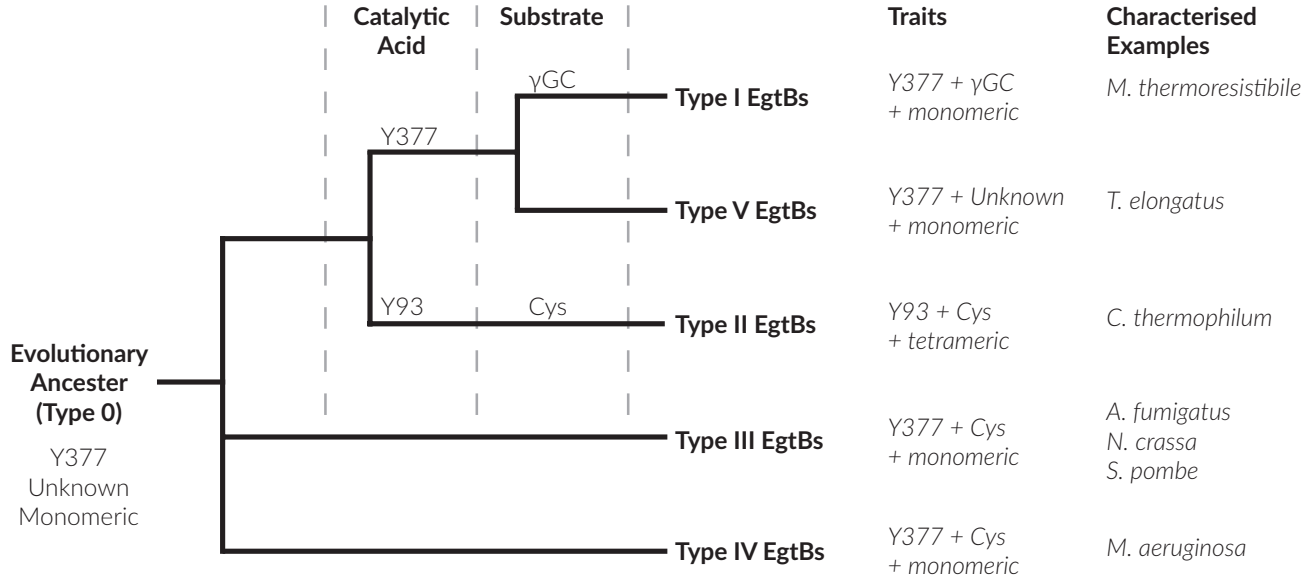

B

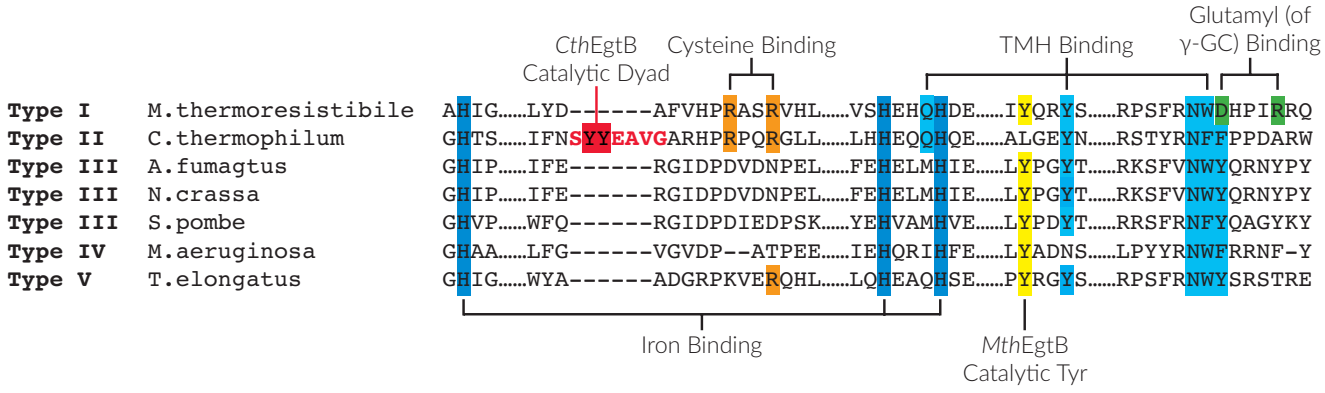

Figure 6. A: A qualitative phylogenetic tree containing characterised EgtB homologs *C. thermophilum*, *M. thermoresistibile*[1, 17], *M. aeruginosa*[8] *A. fumigatus*[7], *S. pombe*[6], *N crassa* [9] and uncharacterised *T. Elongatus*. (… = omitted residues; --- = gaps) **B:** Sequence alignment of characterized EgtB homolgoues *C. thermophilum*, *M. thermoresistibile*[1, 17], *M. aeruginosa*[8] *A. fumigatus*[7], *S. pombe*[6], *N crassa* [9] and uncharacterised *T. Elongatus.* Residues highlighted in red indicate active site loop 1 of *Cth*EgtB. Key residues for binding and catalysis are highlighted and labelled.

CONCLUSION

Based on the crystal structure of *Cth*EgtB in complex with iron (II) and TMH we identified Tyr93 and Tyr94 as essential catalytic residues. Mutation of either residue to phenylalanine significantly reduced sulfoxide synthase activity, whereas only the Tyr94Phe mutation affected the enzymes ability to consume cysteine. These different phenotypes, compounded by their different positions in the oxygen binding pocket provide evidence that Tyr93 serves as a proton donor and Tyr94 serves as a hydrogen bond donor, both facilitating the reduction of the initial iron (III) superoxide species. This reduction is the first catalytic step towards sulfoxide production. Comparison with the structure of EgtB from *M. thermoresistibile* (*Mth*EgtB) and with primary sequences of other bacterial and fungal homologs revealed that the class of ergothioneine biosynthetic sulfoxide synthases is characterized by remarkable active site diversity. Detailed characterization of type I - V sulfoxide synthases will provide a powerful approach understand the catalytic mechanism of oxidative C-S bond formation.[1, 17, 19] Finally, the observed diversity indicates that these sulfoxide synthase types may have emerged from an ancestral enzyme with different substrate specificity than any known extant homolog.

ACKNOWLEDGMENT

The authors would like to thank Alice Maurer for HR ESI MS measurements and the Swiss Lightsource SLS (Villigen, Switzerland) for beamtime and support. This project was supported by a starting grant from the European Research Council (ERC-2013- StG 336559).

ASSOCIATED CONTENT

Supporting Information. Detailed descriptions of all experiments, supporting figures (S1 – S12) and tables (S1 – S3) are shown in the supporting information. The Supporting Information is available free of charge as a PDF file on the ACS Publications website.

REFERENCES

1. Goncharenko, K. V.; Vit, A.; Blankenfeldt, W.; Seebeck, F. P., Structure of the Sulfoxide Synthase EgtB from the Ergothioneine Biosynthetic Pathway. *Angew. Chem. Int. Ed. Engl.* **2015,** *54* (9), 2821 - 2824.

2. Seebeck, F. P., In vitro reconstitution of Mycobacterial ergothioneine biosynthesis. *J. Am. Chem. Soc.* **2010,** *132*, 6632-6633.

3. Gao, S. S.; Naowarojna, N.; Cheng, R.; Liu, X.; Liu, P., Recent examples of α-ketoglutarate-dependent mononuclear non-haem iron enzymes in natural product biosyntheses. *Nat. Prod. Rep.* **2018,** *35* (8), 792 - 837.

4. Askari, A.; Melville, D. B., The reaction sequence in ergothioneine biosynthesis: hercynine as an intermediate. *J. Biol. Chem.* **1962,** *237* (5), 1615-&.

5. Hu, W.; Song, H.; Sae Her, A.; Bak, D. W.; Naowarojna, N.; Elliot, S. J.; Qin, L.; Chen, X.; Liu, P., Bioinformatic and Biochemical Characterizations of C−S Bond Formation and Cleavage Enzymes in the Fungus Neurospora crassa Ergothioneine Biosynthetic Pathway. *Org. Lett.* **2014,** *16* (20), 5382 - 5385.

6. Pluskal, T.; Ueno, M.; Yanagida, M., Genetic and Metabolomic Dissection of the Ergothioneine and Selenoneine Biosynthetic Pathway in the Fission Yeast, S. pombe, and Construction of an Overproduction System. *PLoS One* **2014,** *9* (5), e97774.

7. Sheridan, K. J.; Lechner, B. E.; Keeffe, G. O.; Keller, M. A.; Werner, E. R.; Lindner, H.; Jones, G. W.; Haas, H.; Doyle, S., Ergothioneine Biosynthesis and Functionality in the Opportunistic Fungal Pathogen, Aspergillus fumigatus. *Sci Rep.* **2016,** *6*, 35306.

8. Liao, C.; Seebeck, F. P., Convergent Evolution of Ergothioneine Biosynthesis in Cyanobacteria. *Chembiochem* **2017,** *18* (21), 2115 - 2118.

9. Bello, M. H.; Barrera-Perez, V.; Morin, D.; Epstein, L., The Neurospora crassa mutant NcDEgt-1 identifies an ergothioneine biosynthetic gene and demonstrates that ergothioneine enhances conidial survival and protects against peroxide toxicity during conidial germination. *Fungal Genet. Biiol* **2012,** *49* (2), 160-172.

10. Cumming, B. M.; Chinta, K. C.; Reddy, V. P.; Steyn, A. J. C., Role of Ergothioneine in Microbial Physiology and Pathogenesis. *Antioxid. Redox Signal.* **2018,** *28* (6), 431 - 444.

11. Gamage, A. M.; Liao, C.; Cheah, I. K.; Chen, Y.; Lim, D. R. X.; Ku, J. W. K.; Chee, R. S. L.; Gengenbacher, M.; Seebeck, F. P.; Halliwell, B.; Gan, Y. H., The proteobacterial species Burkholderia pseudomallei produces ergothioneine which enhances virulence in mammalian infection. *FASEB, J* **2018,** *11:fj201800716*.

12. Saini, H. S.; Cumming, B. M.; Guidry, L.; Lamprecht, D. A.; Adamson, J. H.; Reddy, V. P.; Chinta, K. C.; Mazorodze, J. H.; Glasgow, J. N.; Richard-Greenblatt, M.; Gomez-Velasco, A.; Bach, H.; Av-Gay, Y.; Eoh, H.; Rhee, K.; Steyn, A. J. C., Ergothioneine Maintains Redox and Bioenergetic Homeostasis Essential for Drug Susceptibility and Virulence of Mycobacterium tuberculosis. *Cell Rep.* **2016,** *14* (3), 572 - 585.

13. Aik, W. S.; McDonough, M. A.; Thalhammer, A.; Chowdhury, R.; Schofield, C. J., Role of the jelly-roll fold in substrate binding by 2-oxoglutarate oxygenases. *Curr. Opin. Struct. Biol.* **2012,** *22* (6), 691 - 700.

14. Meury, M.; Knop, M.; Seebeck, F. P., Structural Basis for Copper-Oxygen Mediated C-H Bond Activation by the Formylglycine-Generating Enzyme. *Angew Chem Int Ed Engl.* **2017,** *56* (27), 8115 - 8119.

15. Dierks, T.; Dickmanns, A.; Preusser-Kunze, A.; Schmidt, B.; Mariappan, M.; von Figura, K.; Ficner, R.; Rudolph, M. G., Molecular Basis for Multiple Sulfatase Deficiency and Mechanism for Formylglycine Generation of the Human Formylglycine-Generating Enzyme. *Cell* **2005,** *121* (4), 541-552.

16. Newton, G. L.; Leuung, S. S.; Wakabayashi, J. L.; Rawat, M.; Fahey, R. C., The DinB Superfamily Includes Novel Mycothiol, Bacillithiol, and Glutathione S-Transferases. *Biochemistry* **2011,** *50* (49), 10751-10760.

17. Goncharenko, K. V.; Seebeck, F. P., Conversion of a non-heme iron-dependent sulfoxide synthase into a thiol dioxygenase by a single point mutation. *Chem. Commun.* **2016,** *52* (9), 1945 - 1948.

18. Braunshausen, A.; Seebeck, F. P., Identification and characterization of the first ovothiol biosynthetic enzyme. *J. Am. Chem. Soc.* **2011,** *133* (6), 1757-1759.

19. Chen, L.; Naowarojna, N.; Song, H.; Wang, S.; Wang, J.; Deng, Z.; Zhao, C.; P., L., Use of a tyrosine analog to modulate the two activities of a non-heme iron enzyme OvoA in ovothiol biosynthesis, cysteine oxidation versus oxidative C-S bond formation. *J. Am. Chem. Soc.* **2018,** *140* (13), 4604 - 4612.

20. Faponle, A. S.; Seebeck, F. P.; de Visser, S. P., Sulfoxide Synthase versus Cysteine Dioxygenase Reactivity in a Nonheme Iron Enzyme. *J. Am. Chem. Soc.* **2017,** *139* (27), 9259 - 9270.

21. Wei, W. J.; Siegbahn, P. E.; Liao, R. Z., Theoretical Study of the Mechanism of the Nonheme Iron Enzyme EgtB. *Inorg. Chem.* **2017,** *56* (6), 3589 - 3599.

22. Tian, G.; Su, H.; Liu, Y., Mechanism of Sulfoxidation and C−S Bond Formation Involved in the Biosynthesis of Ergothioneine Catalyzed by Ergothioneine Synthase (EgtB). *ACS Catalysis* **2018,** *8*, 5875 - 5889.

23. Kulik, H. J.; Blasiak, L. C.; Marzari, N.; Drennan, C. L., First-Principles Study of Non-heme Fe(II) Halogenase SyrB2 Reactivity. *Journal of the American Chemical Society* **2009,** *131* (40), 14426-14433.

24. Blasiak, L. C.; Vaillancourt, F. H.; Walsh, C. T.; Drennan, C. L., Crystal structure of the non-haem iron halogenase SyrB2 in syringomycin biosynthesis. *Nature* **2006,** *440* (7082), 368-371.

25. Song, H.; Her, A. S.; Raso, F.; Zheng, Z.; Huo, Y.; Liu, P., Cysteine Oxidation Reactions Catalyzed by a Mononuclear Nonheme Iron Enzyme (OvoA) in Ovothiol Biosynthesis. *Org. Lett.* **2014,** *16* (8), 2122-2125.

26. Mbughuni, M. M.; Chakrabarti, M.; Hayden, J. A.; Bominaar, E. L.; Hendrich, M. P.; Münck, E.; Lipscomb, J. D., Trapping and spectroscopic characterization of an FeIII-superoxo intermediate from a nonheme mononuclear iron-containing enzyme. *Proc. Natl. Acad. Sci. U. S. A.* **2010,** *107* (39), 16788 - 16793.

27. Zhu, H.; Peck, S. C.; Bonnot, F.; van der Donk, W. A.; Klinman, J. P., Oxygen-18 Kinetic Isotope Effects of Nonheme Iron Enzymes HEPD and MPnS Support Iron(III) Superoxide as the Hydrogen Abstraction Species. *J. Am. Chem. Soc.* **2015,** *137* (33), 10448 - 10451.

28. Hong, S.; Sutherlin , K. D.; Park, J.; Kwon, E.; Siegler, M. A.; Solomon, E. I.; Nam, W., Crystallographic and spectroscopic characterization and reactivities of a mononuclear non-haem iron(III)-superoxo complex. *Nat. Commun.* **2014,** *5*, 5440.

29. van der Donk, W. A.; Krebs, C.; Bollinger Jr., J. M., Substrate activation by iron superoxo intermediates. *Curr. Opin. Stuct. Biol.* **2010,** *20*, 1- 11.

30. Xing, G.; Diao, Y.; Hoffart, L. M.; Barr, E. W.; Prabhu, S.; Arner, R. J.; Reddy, C. C.; Krebs, C.; Bollinger Jr., J. M., Evidence for C-H cleavage by an iron-superoxide complex in the glycol cleavage reaction catalyzed by myo-inositol oxygenase. *Proc. Natl. Acad. Sci. U. S. A.* **2006,** *103* (16), 6130 - 6135.

31. Tamanaha, E.; Zhang, B.; Guo, Y.; Chang, W. C.; Barr, E. W.; Xing, G.; St Clair, J.; Ye, S.; Neese, F.; Bollinger, J. M. J.; Krebs, C., Spectroscopic Evidence for the Two C-H-Cleaving Intermediates of Aspergillus nidulans Isopenicillin N Synthase. *J. Am. Chem. Soc.* **2016,** *138* (28), 8862 - 8874.

32. Vit, A.; Mashabela, G. T.; Blankenfeldt, W.; Seebeck, F. P., Structure of the Ergothioneine-Biosynthesis Amidohydrolase EgtC. *ChemBioChem* **2015,** *16* (10), 1490 - 1496.

33. Joseph, C. A.; Maroney, M. J., Cysteine dioxygenase: structure and mechanism. *Chem. Commun.* **2007,** (32), 3338-3349.

34. Gardner, J. D.; Pierce, B. S.; Fox, B. G.; Brunold, T. C., Spectroscopic and Computational Characterization of Substrate-Bound Mouse Cysteine Dioxygenase: Nature of the Ferrous and Ferric Cysteine Adducts and Mechanistic Implications. *Biochemistry* **2010,** *49*, 6033-6041.

35. Kumar, D.; Thiel, W.; de Visser, S. P., Theoretical study on the mechanism of the oxygen activation process in cysteine dioxygenase enzymes. *J. Am. Chem. Soc.* **2011,** *133*, 3869 - 3882.

36. Ye, S.; Wu, X.; Wei, L.; Tang, D.; Sun, P.; Bartlam, M.; Rao, Z., An insight into the mechanism of human cysteine dioxygenase. Key roles of the thioether-bonded tyrosine-cysteine cofactor. *J. Biol. Chem.* **2007,** *282* (5), 3391 - 3402.

37. Mantri, M.; Zhang, Z.; McDonough, M. A.; Schofield, C. J., Autocatalysed oxidative modifications to 2-oxoglutarate dependent oxygenases. *FEBS J.* **2012,** *279* (9), 1563 - 1575.

38. Yan, W.; Song, H.; Song, F.; Guo, Y.; Wu, C. H.; Her, A. S.; Pu, Y.; Wang, S.; Naowarojna, N.; Weitz, A.; Hendrich, M. P.; Costello, C. E.; Zhang, L.; Liu, P.; Zhang, Y. J., Endoperoxide formation by an α-ketoglutarate-dependent mononuclear non-haem iron enzyme. *Nature* **2015,** *527* (7579), 539 - 543.

39. Ryle, M. J.; Liu, A.; Muthukumaran, R. B.; Ho, R. Y.; Koehntop, K. D.; McCracken, J.; Que, L. J.; Hausinger, R. P., O2- and alpha-ketoglutarate-dependent tyrosyl radical formation in TauD, an alpha-keto acid-dependent non-heme iron dioxygenase. *Biochemistry* **2003,** *42* (7), 1854 - 1862.

40. Dominy, J. E. J.; Hwang, J.; Guo, S.; Hirschberger, L. L.; Zhang, S.; Stipanuk, M. H., Synthesis of amino acid cofactor in cysteine dioxygenase is regulated by substrate and represents a novel post-translational regulation of activity. *J. Biol. Chem.* **2008,** *283* (18), 12188 - 12201.

41. Timmins, A.; Saint-André, M.; de Visser, S. P., Understanding How Prolyl-4-hydroxylase Structure Steers a Ferryl Oxidant toward Scission of a Strong C-H Bond. *J. Am. Chem. Soc.* **2017,** *139* (29), 9855 - 9866.

42. Todd, A. E.; Orengo, C. A.; Thornton, J. M., Plasticity of enzyme active sites. *Trends Biochem. Sci.* **2002,** *27* (8), 419-426.

43. Todd, A. E.; Orengo, C. A.; Thornton, J. M., Evolution of function in protein superfamilies, from a structural perspective1. *Journal of Molecular Biology* **2001,** *307* (4), 1113-1143.

44. Schrag, J. D.; Winkler, F. K.; Cygler, M., Pancreatic lipases: Evolutionary intermediates in a positional change of catalytic carboxylates? *Journal of Biological Chemistry* **1992,** *267* (7), 4300-4303.

45. Hasson, M. S.; Schlichting, I.; Moulai, J.; Taylor, K.; Barrett, W.; Kenyon, G. L.; Babbitt, P. C.; Gerlt, J. A.; Petsko, G. A.; Ringe, D., Evolution of an enzyme active site: The structure of a new crystal form of muconate lactonizing enzyme compared with mandelate racemase and enolase. *Proc Natl Acad Sci U S A.* **1998,** *95* (18), 10396-10401.

46. Wilce, M. C. J.; Board, P. G.; Feil, S. C.; Parker, M. W., Crystal structure of a theta-class glutathione transferase. *EMBO Journal* **1995,** *14* (10), 2133-2143.

47. Skirgaila, R.; Grazulis, S.; Bozic, D.; Huber, R.; Siksnys, V., Structure-based redesign of the Catalytic/Metal binding site of Cfr 10I restriction endonuclease reveals importance of spatial rather than sequence conservation of active centre residues1. *J. Mol. Biol.* **1998,** *279* (2), 473-481.

48. Giger, L.; Caner, S.; Obexer, R.; Kast, P.; Baker, D.; Ban, N.; Hilvert, D., Evolution of a designed retro-aldolase leads to complete active site remodeling. *Nat. Chem. Biol.* **2013,** *9* (8), 494-498.

49. Song, H.; Leninger, M.; Lee, N.; Liu, P., Regioselectivity of the Oxidative C–S Bond Formation in Ergothioneine and Ovothiol Biosyntheses. *Org. Lett.* **2013,** *15* (18), 4854 - 4857.

TOC